



Neutrino Process in Core-collapse Supernovae with Neutrino Self-interaction and MSW Effects

Heamin Ko¹, Myung-Ki Cheoun¹ , Eunja Ha¹, Motohiko Kusakabe² , Takehito Hayakawa³, Hirokazu Sasaki⁴, Toshitaka Kajino^{2,4} , Masa-aki Hashimoto⁵, Masaomi Ono⁶ , Mark D. Usang⁷, Satoshi Chiba⁷, Ko Nakamura⁸ ,

Alexey Tolstov⁹ , Ken'ichi Nomoto⁹ , Toshihiko Kawano¹⁰, and Grant J. Mathews¹¹

¹ Department of Physics and OMEG institute, Soongsil University, Seoul 07040, Republic of Korea; cheoun@ssu.ac.kr

² School of Physics and International Research Center for Big-Bang Cosmology and Element Genesis, Beihang University, Beijing 100083, People's Republic of China

³ National Institutes for Quantum and Radiological Science and Technology, 2-4 Shirakata, Tokai, Naka, Ibaraki 319-1106, Japan

⁴ The University of Tokyo, Bunkyo-ku, Tokyo 113-0033, Japan and National Astronomical Observatory of Japan, Mitaka, Tokyo 181-8588, Japan

⁵ Kyushu University, Hakozaki, Fukuoka 812-8581, Japan

⁶ RIKEN, 2-1 Hirosawa, Wako-shi, Saitama 351-0198, Japan

⁷ Tokyo Institute of Technology, 2-12-1 Ookayama, Meguro, Tokyo 113-0033, Japan

⁸ Fukuoka University, 8-19-1 Nanakuma, Jonan-ku, Fukuoka 814-0180, Japan

⁹ Kavli Institute for the Physics and Mathematics of the Universe (WPI), The University of Tokyo, 5-1-5 Kashiwanoha, Kashiwa, Chiba 277-8583, Japan

¹⁰ Theoretical Division, Los Alamos National Laboratory, Los Alamos, NM 87545, USA

¹¹ Department of Physics, Center for Astrophysics, University of Notre Dame, Notre Dame, IN 46556, USA

Received 2020 January 12; accepted 2020 February 18; published 2020 March 4

Abstract

We calculate the abundances of ⁷Li, ¹¹B, ⁹²Nb, ⁹⁸Tc, ¹³⁸La, and ¹⁸⁰Ta produced by neutrino (ν)-induced reactions in a core-collapse supernova explosion. We consider the modification by ν self-interaction (ν -SI) near the neutrinosphere and the Mikheyev–Smirnov–Wolfenstein (MSW) effect in the outer layers based on time-dependent neutrino energy spectra. Abundances of ⁷Li and the heavy isotopes ⁹²Nb, ⁹⁸Tc, and ¹³⁸La are reduced by a factor of 1.5–2.0 by the ν -SI. In contrast, ¹¹B is relatively insensitive to the ν -SI. We find that the abundance ratio of heavy to light nuclei, ¹³⁸La/¹¹B, is sensitive to the neutrino mass hierarchy, and the normal mass hierarchy is more likely to be consistent with the solar meteoritic abundances.

Unified Astronomy Thesaurus concepts: [Supernova neutrinos \(1666\)](#); [Explosive nucleosynthesis \(503\)](#); [Neutrino oscillations \(1104\)](#)

1. Introduction

The neutrino (ν)-process is the nucleosynthesis mechanism induced by the neutrinos produced in core-collapse supernova (CCSN) explosions (Woosley et al. 1990; Heger et al. 2005). It is a unique nucleosynthesis process that only affects the abundances of some rare nuclei, such as ⁷Li and ¹¹B (Yoshida et al. 2005, 2006), ¹⁹F (Kobayashi et al. 2011), ⁹²Nb (Hayakawa et al. 2013), ⁹⁸Tc (Hayakawa et al. 2018), ¹³⁸La, and ¹⁸⁰Ta (Heger et al. 2005; Hayakawa et al. 2010; Wu et al. 2015). A comparison of calculated ν -process abundances with observational abundances or meteoritic analyses can provide valuable information about the associated ν physics and CCSN physics (Heger et al. 2005; Austin et al. 2011; Mathews et al. 2012; Tamborra et al. 2014; Sieverding et al. 2018; Abbar et al. 2019; Glas et al. 2019). For example, recent meteoritic analyses have revealed ratios at the solar system formation of ⁹²Nb/⁹³Nb $\simeq 10^{-5}$ (Iizuka et al. 2016) and ⁹⁸Tc/⁹⁸Ru $< 6 \times 10^{-5}$ (Becker & Walker 2003). These ratios can be used as nuclear cosmochronometers for the duration from the last supernova (SN) to the time of the solar system formation (Hayakawa et al. 2013, 2018). Previous studies (Heger et al. 2005; Yoshida et al. 2005; Wu et al. 2015) have also shown that the ν -process isotopic abundances are sensitive to neutrino energy spectra, and consequently the ν -process is a probe of the neutrino physics. Because each ν -process isotope is predominantly produced by one or two ν -induced reactions (Hayakawa et al. 2018), its abundance is more sensitive to neutrino energy spectra rather than other nucleosynthesis mechanisms.

However, there still remain some ambiguities in treating the ν physics in CCSNe. One example is the ν mass hierarchy (MH), i.e., the normal hierarchy (NH) versus the inverted hierarchy (IH). The neutrino MH strongly affects the ν -flux and the subsequently produced ν -process abundances (Yoshida et al. 2006). Another is the matter-enhanced ν oscillation, i.e., the Mikheyev–Smirnov–Wolfenstein (MSW) effect that gives rise to additional ν mixing from that of free space around the bottom of the C/O-rich layer (Yoshida et al. 2005, 2006). The third important aspect is the ν self-interaction (ν -SI) arising from nonlinear ν - ν scattering (Sigl & Raffelt 1993; Serreau & Volpe 2014; Chakraborty et al. 2016; Sawyer 2016; Dasgupta et al. 2017; Tamborra et al. 2017).

This is usually negligible, but near to the neutrinosphere the ν -density approaches $\sim 10^{32}$ cm⁻³ (Pehlivan et al. 2011). This density is large enough that the ν -SI should be taken into account for the estimation of the ν -flux.

A previous study (Wu et al. 2015) calculated the ν -process and νp -process considering the ν -SI and MSW effects; it was found that the abundances of ¹³⁸La and ¹⁸⁰Ta are enhanced by the ν -SI effect but the νp -process is not sensitive to this effect. Also, the ν -SI effect on the νp -process has been studied by including multi-angle three-flavor mixing (Sasaki et al. 2017). In this Letter, we report on a new systematic investigation of the ν -process that takes into account both the ν -SI effect calculated from Sasaki et al. (2017) and the MSW effect. We also discuss the MH dependence of the heavy-to-light isotopic abundances.

2. Neutrino Spectra

All of the modifications due to the ν -SI and the matter effect in the propagating ν -flux can be accounted for by solving the following evolution equation for the $\nu(\vec{r})$ -density matrix (Sigl & Raffelt 1993; Serreau & Volpe 2014)

$$i \dot{\rho}_{\mathbf{p}}(\dot{\rho}_{\mathbf{p}}) = +(-) \frac{1}{2E} [M^2, \rho_{\mathbf{p}}(\bar{\rho}_{\mathbf{p}})] + \sqrt{2} G_F [L, \rho_{\mathbf{p}}(\bar{\rho}_{\mathbf{p}})] \\ + \sqrt{2} G_F \Sigma_{\mathbf{q}} (1 - \cos \theta_{\mathbf{p}\mathbf{q}}) [(\rho_{\mathbf{q}} - \bar{\rho}_{\mathbf{q}}), \rho_{\mathbf{p}}(\bar{\rho}_{\mathbf{p}})]. \quad (1)$$

Here, M is the ν mass-matrix including the vacuum oscillations, while \mathbf{p} and \mathbf{q} are the momenta of the propagating and background neutrinos. The ν -density matrix ρ and the charged lepton number density matrix L are given by $\rho_{\alpha\beta} = \sum_{\gamma=e,\mu,\tau} \langle \nu_{\alpha} | \nu_{\gamma}(t) \rangle \langle \nu_{\gamma}(t) | \nu_{\beta} \rangle$ and $L_{\alpha\beta} = (N_{\alpha} - N_{\bar{\alpha}}) \delta_{\alpha\beta}$ with ν flavors α and β . N_{α} denotes the lepton number density and $\delta_{\alpha\beta}$ is the Kronecker delta. The first and second terms on the rhs of Equation (1) describe ν oscillations in vacuum and the matter effect, respectively. The electron density is calculated with a constant electron fraction w.r.t. the baryon density given by a fit (Fogli et al. 2003) to a shock-propagation model. The muon and tau densities are assumed to be negligible in this work. The ν -SI is taken into account in the third term.

To solve Equation (1), we assume a ν -bulb model with multi-angle ν -flavor evolution, azimuthal and time-translational symmetry in a two-flavor neutrino scheme (Raffelt et al. 2013; Abbar & Duan 2015; Dasgupta & Mirizzi 2015). Effects from the violation of these symmetries on the CCSN ν propagation as well as from the asymmetric neutrinosphere (Mirizzi et al. 2016; Abbar et al. 2019) bring about the multi-azimuthal angle (MAA) instability and fast ν -flavor conversion (Abbar et al. 2019; Glas et al. 2019; Delfan Azari et al. 2020). These effects on the ν -process are left for a future study.

The evolution of the ν -flux by the ν -SI is achieved by solving Equation (1) for the ν distribution function, $f(r; \epsilon_{\nu}, T_{\nu_{\alpha}}(t)) = f_{\text{Fermi-Dirac}}(\epsilon_{\nu}, T_{\nu_{\alpha}}(t)) \langle \rho(r; \epsilon_{\nu}) \rangle$, which is normalized with the angle-averaged ν -density matrix $\langle \rho(r; \epsilon_{\nu}) \rangle$. The differential ν -flux is defined as follows:

$$\frac{d}{d\epsilon_{\nu}} \phi_{\nu_{\alpha}}(t, r; \epsilon_{\nu}, T_{\nu_{\alpha}}) = \frac{\mathcal{L}_{\nu_{\alpha}}(t)}{4\pi r^2} \frac{\epsilon_{\nu}^2}{\langle \epsilon_{\nu} \rangle} f(r; \epsilon_{\nu}, T_{\nu_{\alpha}}(t)), \quad (2)$$

where $\mathcal{L}_{\nu_{\alpha}}(t)$ is the luminosity of ν_{α} . We adopt the neutrino luminosity evolution based upon the $20 M_{\odot}$ progenitor numerical CCSN simulations summarized in O'Connor et al. (2018). In that paper it was demonstrated that a variety of independent numerical simulations produce nearly identical neutrino spectra and time evolution. We note that instabilities from the matter convection like the standing accretion shock instability (SASI), as well as from the multi-dimensional hydrodynamics on the neutrino transport leading to lepton-emission self-sustained asymmetry (LESA), are thought to be partially taken into account in the modern numerical simulations around the neutrinosphere (Mirizzi et al. 2016).

Values for the $\mathcal{L}_{\nu_{\alpha}}$ and the averaged energy deduced at $t = 50, 100, 200, 300,$ and 500 ms (O'Connor et al. 2018) are given in Table 1. We do not consider the early neutrino burst $t < 50$ ms and assume an exponential decay in the ν -luminosity after 500 ms.

Table 1

Time Evolution of the Luminosity $\mathcal{L}_{\nu_{\alpha}}$ and Effective Energy $\langle E_{\nu_{\alpha}} \rangle$ from the Neutrino Transport Models in O'Connor et al. (2018)

Time (ms)	\mathcal{L}_{ν_e}	$\mathcal{L}_{\bar{\nu}_e}$ (10^{52} erg s $^{-1}$)	\mathcal{L}_{ν_x}	$\langle E_{\nu_e} \rangle$	$\langle E_{\bar{\nu}_e} \rangle$ (MeV)	$\langle E_{\nu_x} \rangle$
50	6.5	6.0	3.6	9.3	12.2	16.5
100	7.2	7.2	3.6	10.5	13.3	16.5
200	6.5	6.5	2.7	13.3	15.5	16.5
300	4.3	4.3	1.7	14.2	16.6	16.5
500	4.0	4.0	1.3	16.0	18.5	16.5

Note. Here $\nu_x = \nu_{\mu}, \nu_{\tau}, \bar{\nu}_{\mu}$ and $\bar{\nu}_{\tau}$.

Note that the \mathcal{L}_{ν_x} becomes weaker than the other luminosities with time while $\langle E_{\nu_x} \rangle$ attains almost a constant effective energy.

The neutrino and electron densities near the neutrinosphere play vital roles during the ν -process in the SN environment. For instance, if the electron density is much larger than the ν -density, it may cause a suppression of the ν -SI effect (Chakraborty et al. 2011). However, as the shock wave propagates, the electron density decreases, so that the flavor change by the ν -SI becomes significant in the outer region (Abbar & Duan 2015). Once the ν -flux is changed by the ν -SI, the flux distributions retain their shapes until they undergo the MSW effect. The baryon matter density in the inner region depends upon the SN model employed. For our purposes, however, it is adequate to adopt the phenomenological model of Fogli et al. (2003; FLMM). Hence, we take a density profile for the inner region approximated as a power law and assume that it remains valid for $t \leq 1$ s. Neutrinos calculated by the FLMN density profile propagate from $r = 10$ to 2000 km with the ν -SI, beyond which no changes occur by the ν -SI.

3. Nucleosynthesis and Abundances

To obtain the temperature and density profiles from the shock propagation we utilize a pre-supernova (pre-SN) model developed for SN1987 (Shigeyama et al. 1988; Blinnikov et al. 2000; Kikuchi et al. 2015). The adopted hydrodynamics model for the SN is constructed with the initial conditions (Blinnikov et al. 2000) selected to reproduce the light curve of SN 1987A. This model is for a $16.2 M_{\odot}$ progenitor with a $6 M_{\odot}$ He core and a metallicity of $Z = Z_{\odot}/4$. The stellar evolution and nucleosynthesis have been updated as described in Kikuchi et al. (2015). The weak s -process utilizes (n, γ) reaction data (Kawano et al. 2010) for the $A \sim 100$ mass region to obtain pre-SN abundances (Hayakawa et al. 2018). For the ν -process, we adopt a nuclear reaction network (Kusakabe et al. 2019) and employ the previous numerical results (Yoshida et al. 2008) for the ν -nucleus reaction cross sections of the light nuclei. These are calculated in a few-body model for ${}^4\text{He}$ reaction and in a shell-model for ${}^{12}\text{C}$. For the heavy nuclei, ν -induced reactions are calculated in the quasi-particle random phase approximation through many multipole transitions dominated by the Gamow-Teller transition (Cheoun et al. 2010, 2012). Neutrino reaction rates in the SN explosion are calculated as follows:

$$\lambda_{\nu_{\alpha}}(t, r) = \int_0^{\infty} \sum_{\beta=e,\mu,\tau} \frac{d\phi_{\nu_{\beta}}}{d\epsilon_{\nu}}(t - r/c, r = 2000 \text{ km}; \epsilon_{\nu_{\beta}}) \\ \times P_{\nu_{\beta}\nu_{\alpha}}(r; \epsilon_{\nu}) \text{Br}(\epsilon_{\nu}) \sigma_{\nu_{\alpha}}(\epsilon_{\nu}) d\epsilon_{\nu}. \quad (3)$$

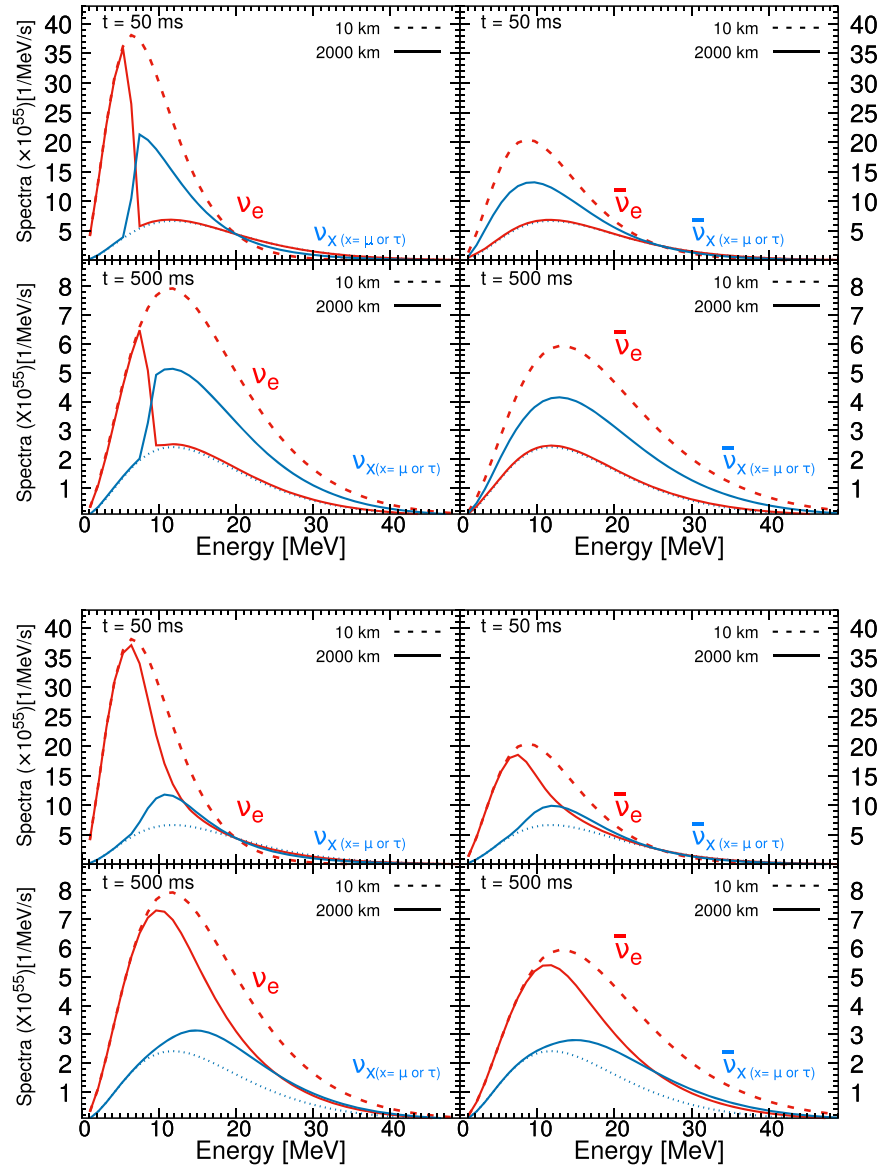


Figure 1. Differential ν -flux ϕ' ($\equiv d\phi/dE$) deduced from the neutrino luminosity \mathcal{L}_{ν_α} (O'Connor et al. 2018) and their modifications by the ν -SI. The upper (lower) panels are for the IH (NH) case for $t = 50$ and 500 ms. The left (right) panels are for ν ($\bar{\nu}$). Dashed and solid lines show the initial flux at 10 km and the final flux at 2000 km after the ν -SI, respectively.

Here the ν reaction cross section, σ_{ν_α} , is multiplied by the branching ratio, $\text{Br}(\epsilon_{\nu'})$, of the excited states calculated using the statistical method (Iwamoto et al. 2016). The flavor transition probability, $P_{\nu_\beta\nu_\alpha}$, includes the ν oscillations in matter based upon the mixing parameters from Tanabashi et al. (2018).

Numerical results of Equation (2) are presented in Figure 1. They show how the ν -flux emitted from the neutrinosphere is modified by the ν -SI. In the IH scheme, the ν_e ($\nu_{x=\mu,\tau}$) flux at 2000 km at $t = 50$ ms is lower (higher) than the original flux from the surface of the neutrinosphere in the energy range from about 6 to 20 MeV. The situation is reversed in the higher energy region above the point of equal flux for the three flavors. However, at $t = 500$ ms, the energy of equal flux becomes higher because of the higher $\langle E_{\nu_e} \rangle$. As a result, the swapping for ν_e and ν_x occurs in a wide energy region above 8 MeV. For anti-neutrinos, the swapping also occurs in a wider energy region (see the right panels in Figure 1). In the NH

scheme, these trends are also observed, but the result for the NH indicates weaker changes in the spectra from the ν -SI. At $t = 50$ ms, the ν_e -flux at 2000 km in the NH scheme is greater than that in the IH scheme. The present result shows that even if the average energies of ν_e and ν_x are identical, in the case that the luminosities of ν_e and ν_x are different, the ν -SI modifies their energy spectra and the final energy spectra depend on the MH.

Figure 2(a) shows the mass fractions of ^{92}Nb , ^{98}Tc , ^{138}La , and ^{180}Ta with and without the ν -SI in each MH scheme. Abundances of ^{92}Nb , ^{98}Tc , and ^{138}La decrease with increasing M_r except for those in the valleys. This trend stems from the neutrino-induced reaction rate, which is proportional to the ν -flux that scales as r^{-2} . A valley around the $M_r \sim 4 M_\odot$ region results from strong destruction via the (n,γ) reactions in heated material behind the shock. Another valley in the region of $M_r < 2.0 M_\odot$ comes from the photodisintegration of the pre-SN elements. Note that the insensitivity of the ^{180}Ta production to the ν -SI comes from the fact that most of the ^{180}Ta is not

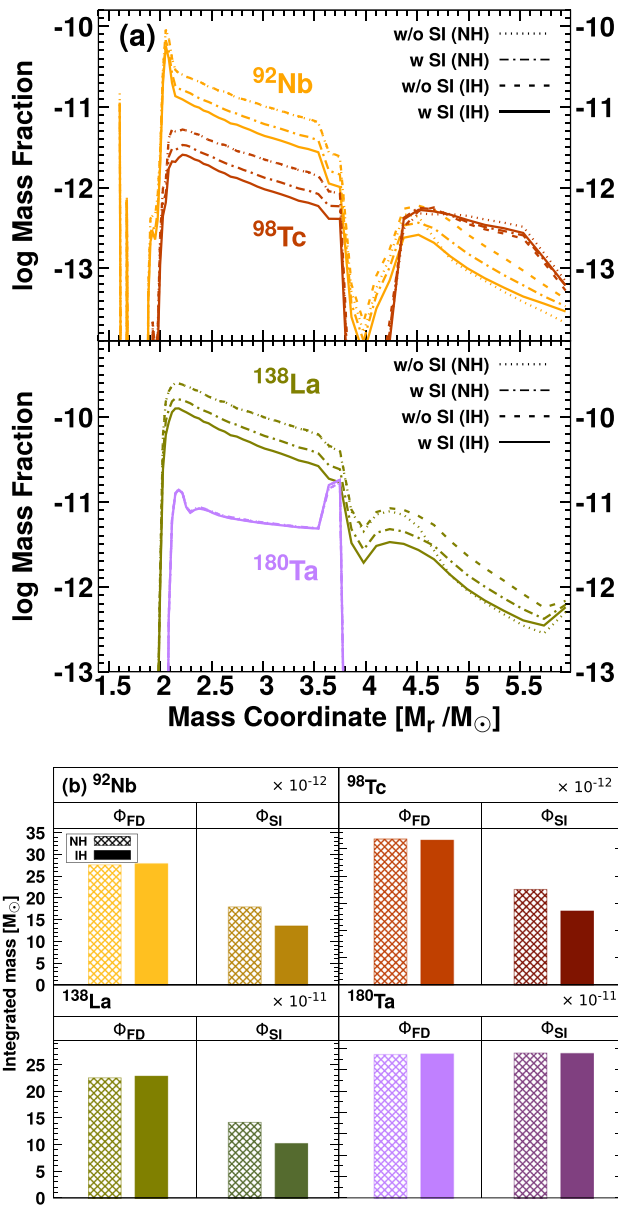


Figure 2. Mass fractions (a) and integrated masses (b) of ^{92}Nb , ^{98}Tc , ^{138}La , and ^{180}Ta abundances in the NH and IH schemes. We show four different cases of w/o SI (NH) (dotted), w/ SI (NH) (dashed-dotted), w/o SI (IH) (dashed), and w/ SI (IH) (solid).

produced via the ν -process in the present model. Because most of the heavy nuclei are produced inside the MSW region, their abundances depend strongly on the ν -SI. We stress that the ν -SI effect decreases the ^{92}Nb , ^{98}Tc , and ^{138}La abundances by a factor of 1.5–2.0 and each final abundance in the NH scheme is larger than that in the IH scheme by about 20%–30%.

These features are explicitly illustrated by the integrated masses in Figure 2(b). This can be understood by the contribution of ν_e . These heavy nuclides are predominantly synthesized by charged current (CC) reactions with ν_e on pre-existing nuclides such as the $^{138}\text{Ba}(\nu_e, e^-)^{138}\text{La}$ reaction and its contribution by ν_e is as large as 70%–90% (Heger et al. 2005; Hayakawa et al. 2018). Thus, the decreased abundances by the ν -SI can be attributed to the decrease of the ν_e -flux.

Even if the average energies of ν_e and ν_x were nearly identical, when the luminosity of ν_e is higher than that of ν_x the

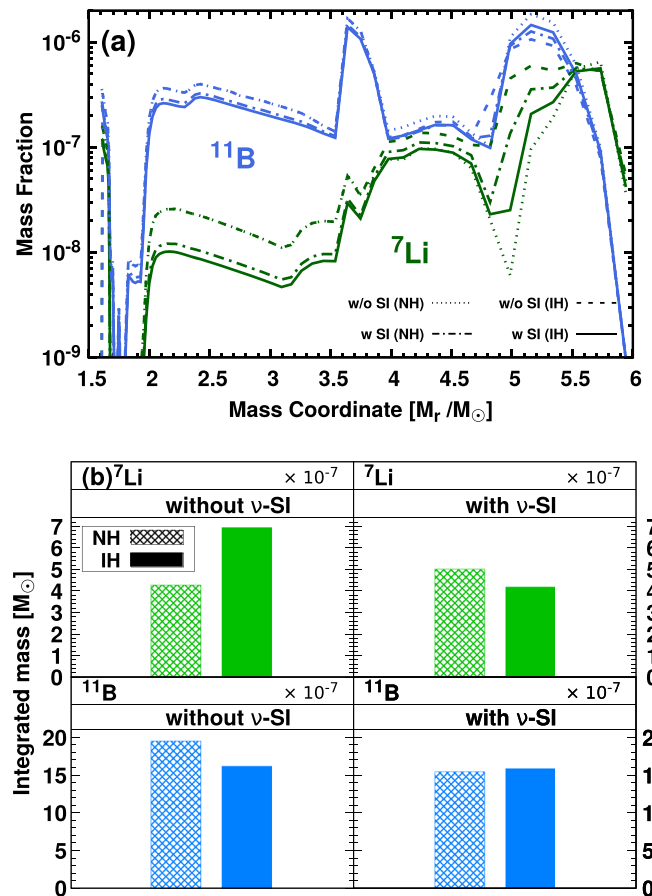


Figure 3. Same as Figure 2, but for ^7Li and ^{11}B . Abundances are plotted at 1 yr after the SN explosion. All results include the MSW effect.

number of ν_e is decreased by the ν -SI, and hence, the ν -process abundances are also decreased.

Figure 3(a) shows the abundances of the light nuclei, ^7Li and ^{11}B , including both the ν -SI and the MSW effect, and their integrated masses are presented in Figure 3(b). The main production regions are the outer region of the MSW layer, 4.7–6.0 M_\odot . The total abundance of ^7Li is much decreased by the ν -SI in the IH scheme, whereas in the NH scheme the ^7Li abundance is slightly increased. ^7Li is produced from ^4He by the ν_e and $\bar{\nu}_e$ via CC reactions as well as neutral current (NC) reactions (Yoshida et al. 2008). The cross sections of the two CC reactions are larger than those of the NC reactions by a factor of 2–3, and the cross section of CC reactions with ν_e is slightly larger than that with $\bar{\nu}_e$ (Yoshida et al. 2008). As a result, the ^7Li abundance is sensitive to the ν_e -flux and the ν -SI effect on ^7Li is similar to that of the heavy isotopes. For example, a nucleosynthesis result for $Z = Z_\odot/4$ (Kusakabe et al. 2019) shows relative contributions from the ν_e CC reactions accounting for 39% (NH) and 24% (IH). Although ^{11}B is also generated by CC reactions with ν_e and $\bar{\nu}_e$ on ^{12}C in addition to NC reactions, these three reactions have contributions on the same order of magnitude (Yoshida et al. 2008). Strictly speaking, the contributions of the CC reactions are subdominant (Kusakabe et al. 2019). Thus, ^{11}B production is relatively insensitive to ν -SI and its abundance decreases by only 5%–10%. In addition, the difference between the IH and NH is only a few percent. A previous study suggested that the abundance ratio $^7\text{Li}/^{11}\text{B}$ is sensitive to the MH (Yoshida et al. 2006). The

${}^7\text{Li}/{}^{11}\text{B}$ ratio is changed by the ν -SI effect from 0.67 to 0.41 in the IH scheme, and from 0.34 to 0.51 in the NH scheme. The ${}^7\text{Li}/{}^{11}\text{B}$ ratio in the NH scheme is larger than that in IH by about 25% in the present model.

Here we discuss the yield ratio of ${}^{138}\text{La}$ and ${}^{11}\text{B}$. The previous study on the ν -process without considering both the ν -SI and the MSW effects (Heger et al. 2005) concluded that enough ${}^{138}\text{La}$ is produced by the ν -process, while the ${}^{11}\text{B}$ is overproduced. The present result shows that the ${}^{138}\text{La}$ abundance is decreased by a factor of about 2, whereas the ${}^{11}\text{B}$ abundance is nearly unaffected by the ν -SI. A ratio of the production factor (PF; Heger & Woosley 2002) of ${}^{138}\text{La}$ to ${}^{11}\text{B}$, $\text{PF}({}^{138}\text{La})/\text{PF}({}^{11}\text{B})$, defined as $\text{PF}[A] = X_A/X_{A\odot}$ with X_A and $X_{A\odot}$ the mass fraction of A in the SNe and in the Sun, respectively, is changed by the ν -SI. The ratio is approximately 0.26 and 0.18 for the NH and IH, respectively; the ratio in the NH scheme is larger than that in the IH scheme by a factor of about 1.4. This large difference originates from the fact that ${}^{138}\text{La}$ is predominantly produced by ν_e but ${}^{11}\text{B}$ production is insensitive to the ν -SI as discussed above. ${}^{138}\text{La}$ is considered to be produced predominantly by the SN ν -process, whereas ${}^{11}\text{B}$ is also produced by cosmic rays.

The ratio can be compared with the expected value $R_{\text{ex}} = f_{\text{metal}} f_{\text{La}}^{\text{SN}}/f_{\text{B}}^{\text{SN}}$. Here $f_{\text{metal}} = Z/Z_{\odot}$ is the normalized metallicity used in this work, which roughly scales with the abundance of ${}^{138}\text{Ba}$, the seed of ${}^{138}\text{La}$ for the ν -process. The quantity $f_{\text{La}}^{\text{SN}} \sim 1$ is the fraction of the solar system abundance of ${}^{138}\text{La}$ originating from SNe, while f_{B}^{SN} is the fraction of ${}^{11}\text{B}$ originating from SNe. This is deduced to be $0.41_{-0.42}^{+0.21}$ by the observed isotopic ratio ${}^{11}\text{B}/{}^{10}\text{B} = (0.7 \pm 0.1)/(0.3 \pm 0.1)$ of cosmic-ray yields (Silberberg & Tsao 1990) and the solar abundance ratio ${}^{11}\text{B}/{}^{10}\text{B} = 3.98$ (Liu et al. 2010). From these values, the ratio is $R_{\text{ex}} = 0.40 - \infty$. Our theoretical values turn out to be more consistent with the NH scheme within 1σ .

This trend originates from the fact that the abundance change by the ν -SI in the IH scheme is stronger than that in the NH scheme. After the ν -SI effect, the ν_e -flux for the NH scheme is higher than that for the IH scheme by a factor of 2–3 (see Figure 1) in the energy range appropriate to ${}^{138}\text{La}$ production (10–20 MeV). As discussed previously, ${}^{138}\text{La}$ production depends strongly on the ν_e -flux. Thus, even if the initial neutrino energy spectra are changed from that assumed here, the trend that the $\text{PF}({}^{138}\text{La})/\text{PF}({}^{11}\text{B})$ ratio after the ν -SI effect in the NH scheme is higher than that in the IH scheme should be preserved.

Finally, we note that recent three-dimensional hydrodynamical SN simulations predicted asymmetric radiation of ν_e and $\bar{\nu}_e$ (Tamborra et al. 2014) and that following studies taking the neutrino angular distribution into account suggest that if the angular distributions of ν_e and $\bar{\nu}_e$ are different, a fast neutrino-flavor transformation by the crossing of ν_e and $\bar{\nu}_e$ occurs (Chakraborty et al. 2016; Sawyer 2016; Dasgupta et al. 2017; Tamborra et al. 2017). Other symmetry violations due to the asymmetric ν -flux and the convection layer can cause the rapid ν flavor conversion than the ν flavor change due to the matter effect. This may happen in the SN neutrinos, and affect the neutrino observation (Abbar et al. 2019; Glas et al. 2019; Delfan Azari et al. 2020) as well as the diffuse SN neutrino background (Mirizzi et al. 2016). In this case, the energy exchange may occur at earlier time and is affected by the larger difference in luminosities between ν_e and ν_x . A hypothetical sterile neutrino may also cause neutrino-flavor changes









between active and sterile species (Ko et al. 2019). This may enhance the MH dependence for the ν -process abundances. However, detailed ν -process calculations with more precise evaluation of the fast ν -conversion effects are beyond of the scope of the present application. This will be addressed in a future work.

4. Conclusion

In conclusion, we have included the effects of both the ν -SI and MSW mixing on the ν -process in CCSN explosions by adopting the numerical results for the time-dependent ν -luminosity and including multi-angle ν -flavor evolution as neutrinos exit the neutrinosphere. When the luminosities of neutrino species are different the ν -SI affects the ν -process abundances, even if the average temperatures of neutrino flavors are the same. The abundances of heavy ν -isotopes and ${}^7\text{Li}$ are reduced by a factor of 1.5–2, whereas ${}^{11}\text{B}$ is decreased by only 5%–10%. The reduction of the ν -isotopic abundances can be systematically understood by the reduction of the ν_e -flux due to the ν -SI. The contribution of CC reactions with ν_e for the production of ${}^7\text{Li}$ and heavy ν -process isotopes is relatively large, whereas for ${}^{11}\text{B}$ the contributions of $\bar{\nu}_e$ and other neutrinos are of the same order as ν_e . Abundance ratios of heavy to light ν -process isotopes such as ${}^{138}\text{La}/{}^{11}\text{B}$ turn out to be more sensitive to the MH, and the present result comparing to the solar abundances shows that the NH scheme is favored. For more definite conclusions, more detailed calculations including the effects from the various asymmetries in the ν -flux around the neutrinosphere are desirable, along with a more refined analysis of relevant meteorite data.

This work was supported by the National Research Foundation of Korea (grant No. NRF-2013M7A1A1075764 and NRF-2017R1E1A1A01074023). This work was supported by Grants-in-Aid for Scientific Research of JSPS (15H03665, 17K05459). M.K. was supported by the visiting scholar program of NAOJ during his stay there. The work of G.J.M. was supported in part by DOE nuclear theory grant DE-FG02-95-ER40934 and in part by the visitor program at NAOJ.

ORCID iDs

Myung-Ki Cheoun  <https://orcid.org/0000-0001-7810-5134>
 Motohiko Kusakabe  <https://orcid.org/0000-0003-3083-6565>
 Toshitaka Kajino  <https://orcid.org/0000-0002-8619-359X>
 Masaomi Ono  <https://orcid.org/0000-0002-0603-918X>
 Ko Nakamura  <https://orcid.org/0000-0002-8734-2147>
 Alexey Tolstov  <https://orcid.org/0000-0002-4587-7741>
 Ken'ichi Nomoto  <https://orcid.org/0000-0001-9553-0685>
 Grant J. Mathews  <https://orcid.org/0000-0002-2663-0540>

References

- Abbar, S., & Duan, H. 2015, *PhLB*, 751, 43
 Abbar, S., Duan, H., Sumiyoshi, K., et al. 2019, *PhRvD*, 100, 043004
 Austin, S. M., Heger, A., & Tur, C. 2011, *PhRvL*, 106, 152501
 Becker, H., & Walker, R. J. 2003, *ChGeo*, 196, 43
 Blinnikov, S., Lundqvist, P., Bartunov, O., et al. 2000, *ApJ*, 532, 1132
 Chakraborty, S., Fischer, T., Mirizzi, A., et al. 2011, *PhRvL*, 107, 151101
 Chakraborty, S., Hansen, R. S., Izaguirre, I., et al. 2016, *JCAP*, 03, 042
 Cheoun, M.-K., Ha, E., Hayakawa, T., et al. 2010, *PhRvC*, 82, 035504
 Cheoun, M.-K., Ha, E., Hayakawa, T., et al. 2012, *PhRvC*, 85, 065807
 Dasgupta, B., & Mirizzi, A. 2015, *PhRvD*, 92, 125030
 Dasgupta, B., Mirizzi, A., & Sen, M. 2017, *JCAP*, 02, 019

- Delfan Azari, M., Yamada, S., Morinaga, T., et al. 2020, *PhRvD*, **101**, 023018
- Fogli, G. L., Lisi, E., Mirizzi, A., et al. 2003, *PhRvD*, **68**, 033005
- Glas, R., Janka, H.-T., Capozzi, F., et al. 2019, arXiv:1912.00274
- Glas, R., Just, O., Janka, H.-T., et al. 2019, *ApJ*, **873**, 45
- Hayakawa, T., Kajino, T., Chiba, S., et al. 2010, *PhRvC*, **81**, 052801
- Hayakawa, T., Ko, H., Cheoun, M.-K., et al. 2018, *PhRvL*, **121**, 102701
- Hayakawa, T., Nakamura, K., Kajino, T., et al. 2013, *ApJL*, **779**, L9
- Heger, A., Kolbe, E., Haxton, W. C., et al. 2005, *PhLB*, **606**, 258
- Heger, A., & Woosley, S. E. 2002, *ApJ*, **567**, 532
- Iizuka, T., Lai, Y.-J., Akram, W., et al. 2016, *E&PSL*, **439**, 172
- Iwamoto, O., Iwamoto, N., Kunieda, S., et al. 2016, *NDS*, **131**, 259
- Kawano, T., Talou, P., Chadwick, M. B., et al. 2010, *J. Nucl. Sci. Technol.*, **47**, 462
- Kikuchi, Y., Hashimoto, M., Ono, M., et al. 2015, *PTEP*, **2015**, 063E0116
- Ko, H., Jang, D., Kusakabe, M., et al. 2019, arXiv:1910.04984
- Kobayashi, C., Izutani, N., Karakas, A. I., et al. 2011, *ApJL*, **739**, L57
- Kusakabe, M., Cheoun, M.-K., Kim, K. S., et al. 2019, *ApJ*, **872**, 164
- Liu, M.-C., Nittler, L. R., Alexander, C. M. O., et al. 2010, *ApJL*, **719**, L99
- Mathews, G. J., Kajino, T., Aoki, W., et al. 2012, *PhRvD*, **85**, 105023
- Mirizzi, A., Tamborra, I., Janka, H.-T., et al. 2016, *NCimR*, **39**, 1
- O'Connor, E., Bollig, R., Burrows, A., et al. 2018, *JPhG*, **45**, 104001
- Pehlivan, Y., Balantekin, A. B., Kajino, T., et al. 2011, *PhRvD*, **84**, 065008
- Raffelt, G., Sarikas, S., & de Seixas, D. S. 2013, *PhRvL*, **111**, 091101
- Sasaki, H., Kajino, T., Takiwaki, T., et al. 2017, *PhRvD*, **96**, 043013
- Sawyer, R. F. 2016, *PhRvL*, **116**, 081101
- Serreau, J., & Volpe, C. 2014, *PhRvD*, **90**, 125040
- Shigeyama, T., Nomoto, K., & Hashimoto, M. 1988, *A&A*, **196**, 141
- Sieverding, A., Martínez-Pinedo, G., Huther, L., et al. 2018, *ApJ*, **865**, 143
- Sigl, G., & Raffelt, G. 1993, *NuPhB*, **406**, 423
- Silberberg, R., & Tsao, C. H. 1990, *PhR*, **191**, 351
- Tamborra, I., Hanke, F., Janka, H.-T., et al. 2014, *ApJ*, **792**, 96
- Tamborra, I., Hüdepohl, L., Raffelt, G. G., et al. 2017, *ApJ*, **839**, 132
- Tanabashi, M., Hagiwara, K., Hikasa, K., et al. 2018, *PhRvD*, **98**, 030001
- Woosley, S. E., Hartmann, D. H., Hoffman, R. D., et al. 1990, *ApJ*, **356**, 272
- Wu, M.-R., Qian, Y.-Z., Martínez-Pinedo, G., et al. 2015, *PhRvD*, **91**, 065016
- Yoshida, T., Kajino, T., & Hartmann, D. H. 2005, *PhRvL*, **94**, 231101
- Yoshida, T., Kajino, T., Yokomakura, H., et al. 2006, *PhRvL*, **96**, 091101
- Yoshida, T., Suzuki, T., Chiba, S., et al. 2008, *ApJ*, **686**, 448